





# Empirical Scrutiny of Geopolymer Concrete Containing Locally Produced Superplasticizer under Varied Temperatures

Lucia Omolayo Agashua<sup>1</sup>✉ , Chinwuba Arum<sup>1,2</sup> , Bamitale Dorcas Oluyemi-Ayibiowu<sup>1</sup>  and Catherine Mayowa Ikumapayi<sup>1</sup> 

<sup>1</sup>Civil and Environmental Engineering Department, Federal University of Technology Akure, 340252, Nigeria

<sup>2</sup>Civil and Mining Engineering Department, JEDS Campus, University of Namibia, Namibia

✉Corresponding author's Email: [agashualight@gmail.com](mailto:agashualight@gmail.com)

## ABSTRACT

Cement manufacturing companies contribute greatly to carbon-dioxide emission during production, hence there is need for novel eco-friendly or biodegradable cementitious material, which has the same strength and also durable. Geopolymers which are eco-friendly waste materials, which can also reduce construction cost, are therefore considered for this purpose. The geopolymer stabilizing materials, fly ash (FA), kaolin clays powder (KCP), rice husk ash (RHA), and alkaline activator (procured sodium silicate, waste-created sodium silicate and sodium hydroxide) were added at 0, 2.5, 5, 7.5, and 10%, to the naturally created superplasticizer geopolymer concrete (GPC), so as to solve the problem of workability and efflorescence associated with fly ash based GPC. FTIR results shows major absorbance band at the region between 950 and 3250  $\text{cm}^{-1}$ . It means that addition of the naturally made superplasticizer to the geopolymer concrete lowered the viscosity and increased the flow behavior of concrete. The geopolymer concrete consists of super plasticizer (1.5%) and optimum of various binders i.e. 5% FA + 7.5% KC + 10% RHA + aggregate + water. At temperature above 70°C both compressive strength and weight decreases, for naturally made and purchased sodium silicate. The optimal geopolymer product showed substantial strength and durability enhancements at 70°C temperatures, with strength and durability values decline above 70°C, indicating material deterioration. A positive correlation between hot-state temperature, strength and durability properties was also established. The  $R^2$  of the Feret on the test set reaches 0.967, indicating its excellent predictive performance.

**Keywords:** Rice Husk, Fourier Transform Infrared Spectroscopy, Waste-created sodium silicate, Superplasticizer; Eco-friendly

## INTRODUCTION

Material for both structural and non-structural concrete applications around the globe It is also known as alkali-activated cement, inorganic polymer concrete, and geocement (Agashua et al., 2023; Abdelli et al., 2017; Adeshokan and Arum, 2023). GPC is dual face materials that combine strong alkaline solutions as activator as well as aluminosilicate materials as binders (Agashua et al., 2023; Obebe et al., 2023). Highly oxidize to corrosion and fire substances, shrinks below convectional concrete, has excellent durability, high compressive, tensile and flexural strengths. There are abundant raw materials which exist for the creation of geopolymers from industrial as well as natural minerals trashes. Besides, its synthesis process guzzles much less energy, particularly those created from industrial rubishes (Omotayo and Arum, 2022; Agashua and Ogiye, 2018; Pelisser et al., 2021). The aluminosilicates can be sourced from numerous pozzolanic materials which possess ample quantities of

silica together with alumina which are mostly rubishes from industrial or agrarian debris for instances ground granulated blast furnace slag (GGBFS), bagasse ash (BA), fly ash (FA), rice husk ash (RHA), palm oil fuel ash (POFA) Kaolin clay and that are used to lessen contaminant impact from natural resources consumption (Abdelli et al., 2017; Phoo-ngernkham et al., 2017; Samantasinghar and Singh, 2020; Rui et al., 2024). This agronomic and industrial debris are utilized individually or blended to serve as the aluminosilicate source in creating geopolymers for sustainable construction (Samantasinghar and Singh, 2020). While, alkaline activators are the second decisive constituent of GPC needed to reacts and polymerizing the aluminosilicates silica together with alumina contents presents in the aluminosilicate (Arum et al., 2022; Babatola and Arum, 2020; Chouhan et al., 2018). These are strong alkaline solutions like  $\text{K}_2\text{SiO}_3$ , (potassium silicate),  $\text{NaOH}$  (sodium hydroxide), as well as  $\text{Na}_2\text{SiO}_3$  (sodium silicate), or combination of these

**RESEARCH ARTICLE**  
 PII: S225204302400026-14  
 Received: June 25, 2024  
 Revised: September 02, 2024  
 Accepted: September 05, 2024

hydroxides and silicates for reacting aluminium (Al) as well as silicon (Si) atoms. More, the geopolymerization procedure depends solely on the reactivity together with concentration of alkaline activator with a lesser quantity of water to binder ratio (Adeshokan and Arum, 2023; Cong and Cheng, 2021; Dewi et al., 2018; Faluyi et al., 2021; Hassan et al. 2019). However, curing temperature of geopolymer concrete results in high early strength but causes a porous geopolymer mix, which reduces the strength at later age (Jindal and Sharma, 2020). This reduction in strength at greater temperatures is owing to early and swift evaporation of water, which not only disturbs the geopolymerization process, but also increases porosity (Shill et al., 2020). Thus, this research evaluated the behaviour of geopolymer concrete created via class-F fly ash, kaolin clay, and rice husk ash as binder and NaOH and Na<sub>2</sub>SiO<sub>3</sub> as alkaline activator.

**Materials and process of geopolymer concrete**

Materials utilized in this experiment were river sand, sodium hydroxide, kaolin clay, crushed granite, factory-created sodium silicate, Portland cement, naturally made sodium silicate as well as super plasticizer, and drinkable water. Further, the GP concrete was thoroughly mixed and Four sets of fly ash based geopolymer concrete was produced which are control concrete, Partially replaced GPC using factory-produced sodium silicate, Partially replaced GPC using laboratory-produced sodium silicate and GPC using laboratory-produced sodium silicate with laboratory-created superplasticizer (LCS) (Table 1). Then workability and strength test were carried out on the four categories of samplings created. Chemical analysis on selected binders (kaolin clay, fly ash and rice husk ash), alkaline activators (sodium silicate and sodium hydroxide) and geopolymer concrete were carried out in the laboratory of Chemical and Material as illustrated in Figures 1 and 2.

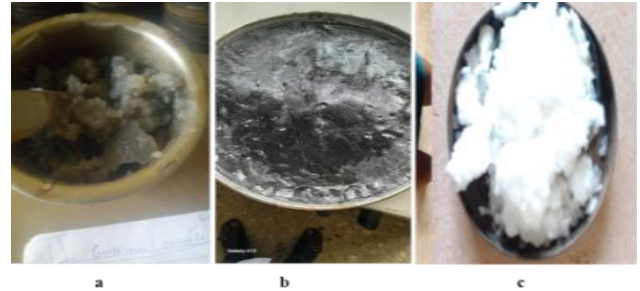


**Figure 1.** I (a and b) Water curing of geopolymer concrete, c) Air drying of geopolymer concrete and II) Alkaline activator (NaOH and Na<sub>2</sub>SiO<sub>3</sub>), b) laboratory-produced Na<sub>2</sub>SiO<sub>3</sub>, and c) NaOH.



**Figure 2.** I= a) Geopolymer concrete using each binders and super plasticizer separately; b) Demolding of different geopolymer using each binders and super plasticizer after 48 hours casting, and c) geopolymer made using optimum values obtained from each binders. II= a) Cement; b) laboratory-created super plasticizer (from rice husk) and c) Fly ash, rice husk ash as well as kaolin clay.



Physical, strength and durability tests were done in the Nigerian Building and Road Research Institute (NBRRI) Jabi Abuja and Federal Ministry of Works (FMW), concrete and pavement unit Sheda Abuja. The GP concretes were cast and removed from the moulds after 24 hours, and cured in water between 7 to 56 days. The design of geopolymer concrete in this research is presented in Figure 3.

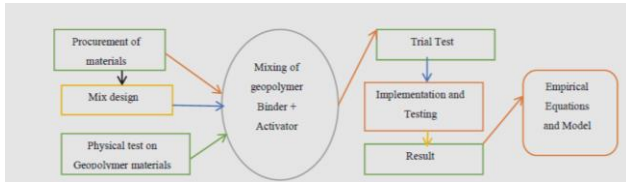


Figure 3. Design process of geopolymer concrete.

## RESULTS AND DISCUSSION

### Outcome of Fourier transform infrared spectroscopy (FTIR) scrutiny

FTIR characterization result for binders ashes is as displayed in Tables 2(a-c). This illustrate that the fly ash has highest key absorbance band at the region between 467.9 and 3695.8  $\text{cm}^{-1}$ . Then, followed by RHA with extreme band of 2084  $\text{cm}^{-1}$  and lower band of 798  $\text{cm}^{-1}$  and the lowest was Kaolin clay with greatest value of 3690  $\text{cm}^{-1}$  and lowest value of 749  $\text{cm}^{-1}$ . Also fly ash notable transmittance between 7.1 and 49.9% was the extreme. The results of FTIR reveal that these binders possess different functional groups namely; alkenes, amides, alkenes, alkynes, acyl chloride and alky halides. An Amine is a type of compound that is derived from ammonia ( $\text{NH}_3$ ), that is amines are derivatives of ammonia. The lower aliphatic amines with a fishy smell are gaseous in nature. Alkynes are traditionally identified as acetylenes, although the term acetylene also denotes  $\text{C}_2\text{H}_2$ , which is an hydrocarbons with single and double carbon-carbon bonds. Fly-ash possesses majorly; Aluminumoxide ( $\text{Al}_2\text{O}_3$ ) at 23.6% as well as Silicon dioxide ( $\text{SiO}_2$ ) at 52.2% and lesser quantity of Iron (III) oxide ( $\text{Fe}_2\text{O}_3$ ) at 7.39%. While, kaolin clay key constituents were 52% of Silicon dioxide ( $\text{SiO}_2$ ) and 35% of Aluminumoxide ( $\text{Al}_2\text{O}_3$ ) together with 2% Potassium oxide ( $\text{K}_2\text{O}$ ) which is insignificant quantity. Likewise, RHA shows significant amount of Silicon dioxide ( $\text{SiO}_2$ ) at 93.3% and Potassium oxide ( $\text{K}_2\text{O}$ ) at 3.40% with insignificant quantity of  $\text{P}_2\text{O}_5$  at 2.1%.

### 1) FTIR Scrutiny for Laboratory-produced Superplasticizer

Fourier transform infrared spectroscopy (FTIR) characterization was employed to investigate the presence of different inorganic and organic bonds in the novel LP superplasticizer and the spectrum obtained is shown in Figure 4. Figure 4 illustrates the major absorbance band at the region between 500 and 3000  $\text{cm}^{-1}$ . The significant peaks which were observed at 617, 707 and 778  $\text{cm}^{-1}$  were attributed to O-Si-O and Si-O-Si bending vibrations

of in situ-synthesized inorganic silicate. Although the intensities of their bands were low compared to those of other bands, their presence confirmed the in situ formation of sodium silicate by the action of sodium hydroxide on inorganic silica from rice husk. On the other hand, one intensified band situated at 1428  $\text{cm}^{-1}$  was a band characteristic of O-C-O stretching vibrations of sodium carbonate, which was believed to originate due to the action of sodium (Na) with atmospheric carbonate. Its high intensity was an indication of the highly reactive nature of sodium to form compounds such as sodium carbonate. The other small diffused bands at 918–1003 and 1251  $\text{cm}^{-1}$  corresponded to Si-O stretching in silicate glasses and weak C-O stretching in native cellulose, respectively.

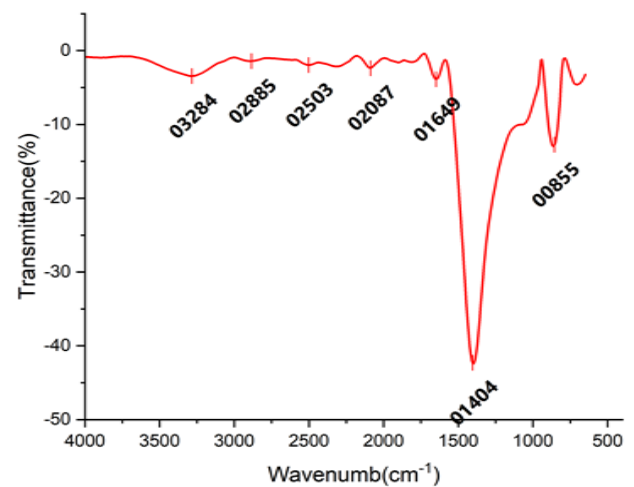
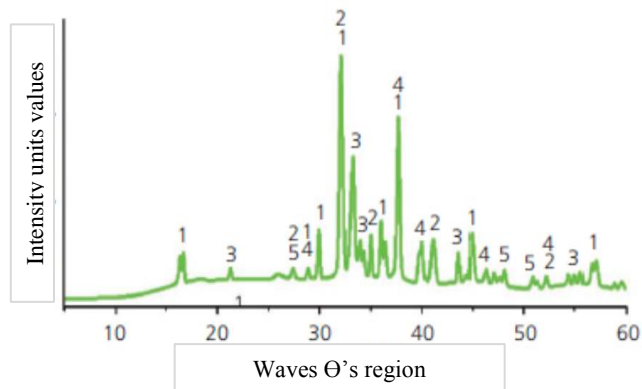


Figure 4. Different vibrational modes in FTIR region obtained for LP superplasticizer.

Some characteristic weak peaks in the LP superplasticizer spectrum at the frequency region of 1650  $\text{cm}^{-1}$  were attributed to quadrant ring stretching in lignin and carbonyl stretching including C=O stretching originating from organic fractions present in the LP superplasticizer, whereas small bands at 2309 and 2900  $\text{cm}^{-1}$  were associated with  $\text{dCH}_2 + \text{dOCH} + \text{dCCH}$  and  $-\text{CH}$  stretching vibrations from fructose and native cellulose. These results again confirmed the XRD results and indicated the formation of inorganic and organic compounds in the LP superplasticizer. Results of FTIR analysis demonstrated that the addition of the LP superplasticizer to the geopolymer concrete lowered the viscosity and increased the flow behavior of concrete, as an effect of the presence of organic fractions in the LP superplasticizer imparted by alkaline digestion of rice husk (Tatal et al., 2020; Silva et al., 2020).

## 2) XRD Scrutiny for laboratory-produced Superplasticizer

The XRD spectrum of the LP superplasticizer is shown in Figure 5, which indicates the presence of a number of peaks with varying intensities.



**Figure 5.** XRD spectrum of novel LP superplasticizer. 1: sodium hydroxide; 2: sodium silicate; 3: native cellulose; 4: b-D-fructose; 5: phenol.

The spectrum shows a broad non-symmetrical hump between 5.2 and 18°  $2\theta$ , indicating the presence of non-crystalline phases and the vitreous nature of the LP superplasticizer. In fact, the vitreous nature actively participated in the geopolymerization reaction and resulted in good mechanical strength of the geopolymeric concrete. The two major inorganic phases reported in the novel LP superplasticizer were sodium silicate ( $\text{Na}_4\text{SiO}_4$ ) and sodium hydroxide. Three minor organic phases originated due to the action of alkali on rice husk, and these were native cellulose ( $\text{C}_6\text{H}_{12}\text{O}_6$ ), b-D-fructose ( $\text{C}_6\text{H}_{12}\text{O}_6$ ) and phenol ( $\text{C}_6\text{H}_6\text{O}$ ). The action of sodium hydroxide on the inorganic silica present on the outer surface of rice husk resulted in the in situ synthesis of sodium silicate, which provided an intense amorphous nature to the developed LP superplasticizer. It is to be noted that sodium silicate acts as a seeding agent for geopolymerization reactions and, in the present study, it was synthesized in situ by the continuous alkaline digestion of rice husk and thus promoted the degree of geopolymerization reactions during the addition of the LP superplasticizer to the concrete mixture. The plasticizing effects were contributed by organic phases in the LP superplasticizer – namely, native cellulose, fructose and phenol. XRD peaks provided strong signals of crystalline cellulose in the LP superplasticizer sample, whereas the amorphous part of the cellulose structure is represented by a broad and less clear diffraction pattern. The evolution of native cellulose in the LP superplasticizer directly indicated the action of

alkali on rice husk during high-temperature alkaline digestion. Due to the complexity of the structures of hemicelluloses and lignin, it is difficult to envisage the complete transformations and rearrangements during alkaline digestion of rice husk, but XRD peaks of the resulting inorganic and organic fractions clearly indicated the action of sodium hydroxide on the rice husk inorganic silica and organic cellulose, hemicellulose and lignin to produce hydrolysis products such as b-D-fructose and phenol in the LP superplasticizer. Furthermore, it is to be pointed out that the commercially available water-reducing organic plasticizers for cement concrete systems perform the function of dispersants into the mixture, where they provide electric repulsion of positive and negative charges and hence the charged cement grains tend to separate from each other to acquire good flowability.

## 3) Scanning electron Microscopy (SEM) of geopolymer materials

SEM was carried out to study the morphology and microstructure of the selected samples (Obebe et al., 2023; Jindal and Sharma, 2020; Muhammad et al., 2019; Palcis, 2023; Shill et al., 2020; Silva et al., 2020). Thus, a comparison between the microstructure of various binders and alkaline activator were conducted and presented in Figures 6 (a-c). Sodium silicate was noticed at  $300 \times 894\mu\text{m}$ ,  $500 \times 536 \mu\text{m}$  and  $3000 \times 268 \mu\text{m}$  and the pulverized RHA was crusted with a platinum coating before performing the experiment, so as to enhance the visibility problem encountered during smooth charge conductivity exact topographic examination. SEM result for RHA also confirmed the result of chemical configuration of RHA by XRF, where at spectrum<sup>-1</sup>, larger quantity of silicon, lesser amount of alumina and oxygen were perceived ascertaining the presence of a large quantity of silica which is in line with result of Phoongerkham, (2017) and Chouhan et al., (2018). Figure 6a for various scanning level displays that most of fly ash particles will form strong bond with the aggregate, and an additional dense gel will also formed if activated. Voids ratio and extended micro cracks will be remarkably decreased because of the dense gel that filled the voids and micro cracks if the binders used in producing geopolymer concrete. The kaolin structure has number of sheets per layer of about 10-50 pieces, size of 1-10  $\mu\text{m}$  and huge quantity of quartz mineral which is the dirtiness of kaolin mineral. Laboratory-produced silicate will cause more homogeneous, compact, and finer microstructure (Figures 6b & c), this is similar to the observation by Dewi et al., 2018, after usage.

**Table 1.** Mix design values for FA-based geopolymer concrete

Mix ID	Molarity	Aggregate (kg/m <sup>3</sup> )		Binders (Kg)				SS/SH Ratio	Density (kg/m <sup>3</sup> )	Water (liter/m <sup>3</sup> )	Age (days)	Slump (mm)
		Fine	Coarse	Cement	Fly	RHA	KC					
A <sub>1</sub>	-	360	720	720	-	-	-	2239	184.2	28	110	
A <sub>2</sub>	12	1080	2160	320	180	120	100	2252	184.7	28	112	
A <sub>3</sub>	12	1080	2160	-	360	180	180	2257	184.2	28	112	
A <sub>4</sub>	12	1080	2160	-	360	180	180	2260	187.4	28	114	

A<sub>1</sub> is control concrete; A<sub>2</sub> is partially replaced geopolymer concrete (GPC); A<sub>3</sub> is GPC using factory-produced sodium silicate and A<sub>4</sub> is GPC using laboratory-produced sodium silicate. SS is sodium silicate; SH is sodium hydroxide; RHA is rice husk ash and KC is kaolin clay.

**Table 2a.** FTIR values for fly ash

Band (cm <sup>-1</sup> )	Transmittance (%)	Functional group
791.8	27.7	Alkenes = CR'R'' s = C-H bend
1635.2	90.9	Alkenes Vw-m C=C Stretch
3695-8	27.4	Amides R-C (O) – NH <sub>2</sub> , w-m N-H Symmetric and asym stretch
3450-3	49.9	Amides R-C (O) – NH <sub>2</sub> , w-m N-H Symmetric and asym stretch
1041-3	7.1	Alkyl halides, R-F Vs C-F Stretch
912-6	32.4	Alkenes RCH = CH <sub>2</sub> , m+ s = C-H bend
467.9	12.2	Alkyl halides R-I, C-I stretch
3623-4	13.4	Amides R-C (O)- NH-R , N-H stretch

FTIR is Fourier transform infrared spectroscopy

**Table 2b.** FTIR values for kaolin clay

Band (cm <sup>-1</sup> )	Transmittance (%)	Functional group
1982.9	101	Alkynes R-C = C-4, medium C=C stretch
3690.1	75.4	Amines – R- NH <sub>2</sub> , N-H symmetric and asym. Stretch, weak
3623	72.5	Amines – R- NH <sub>2</sub> , N-H symmetric and asym. Stretch, weak
1114.5	75.2	Akyl halides R-F, very strongs, C- F stretch
790.2	70.1	Alkenes strong, RCH = R'R C-H band.
749.2	68.2	Alkyl halides R-CL, strong, C-CL stretch.
909.5	30.1	Alkenes, m+s = C-H bend, RCH = CH <sub>2</sub>
998.9	25.0	Alkenes, m+s = C-H bend, RCH = CH <sub>2</sub>

FTIR is Fourier transform infrared spectroscopy and RHA is rice husk ash

**Table 2c.** FTIR values for RHA

Band (cm <sup>-1</sup> )	Transmittance (%)	Functional group
2083.6	98.2	Alkynes R-C = C-H, medium, C= stretch
1982.9	98.0	Alkynes R-C = C-H, medium, C= stretch
1848.8	97.9	Acyl chlorides Ar – C(O) – Cl, C- 0 stretch
797.7	89.7	Alkyl halides intensity, strong, C-CL stretch
1058.6	62.4	Alkyl halides intensity, very strong, C-CF stretch

FTIR is Fourier transform infrared spectroscopy

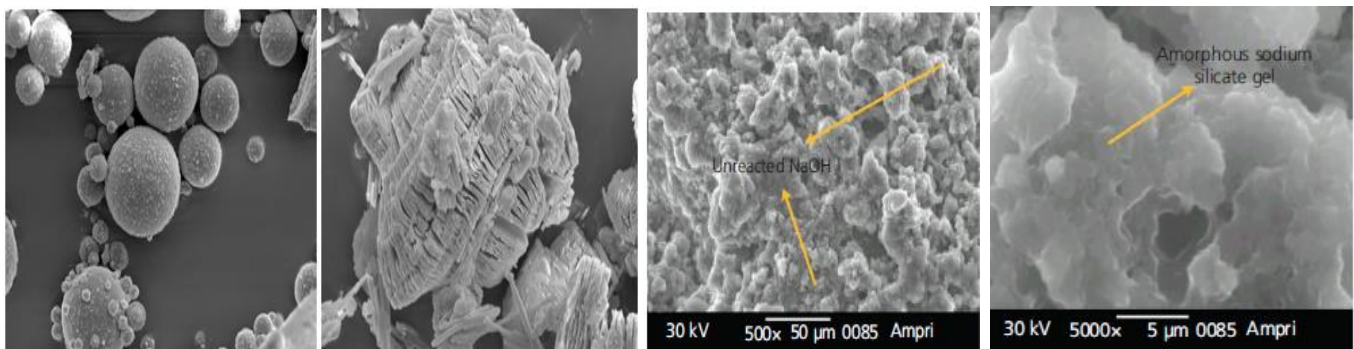


**Figure 6.** a) Morphology of fly ash; b) morphology of kaolin observed; c & d) SEM imageries of laboratory-created superplasticizer at four varied displaying the presence of extremely unstructured sodium silicate gel together with unoxidize sodium hydroxide.

The outcomes of the SEM and FTIR scrutinizes also support the SEM scrutiny.

#### 4) SEM analysis on hardened concrete

SEM was carried out on hardened concrete cured by immersion in 5% sodium sulphate + 5% magnesium sulphate, 5% sodium chloride, 5% sodium sulphate, 3% sulphuric acid and water at 90 days. Comparison between the morphology and microstructure of various immersion were presented in Figures 5-7. Atomic concentrations of geopolymer concrete immersed in water and sodium sulphate solution shows 61.39% and 39.99% respectively for water and sodium sulphate immersion respectively for silicon content, while weight concentration for silicon content also confirm water at 56.31% as highest values, followed by sodium chloride value of 35.27% and least values for both atomic and weight concentration was sulphuric acid immersion with 32.93 and 28.24% respectively (Figures 7 & 8).

Aluminium content followed trend of sodium chloride (22.13% and 18.78%) as the extreme level, and sodium sulphate at 21.96% and 18.57% for both atomic and weight concentration measurement. The lowest immersion level was water (16.37%) and sulphuric acid (13.98%) for atomic and weight concentration respectively. Both atomic and weight concentration measurement for calcium content reveals highest values of 23.52% and 28.78% for sodium chloride immersion and 22.67% and 27.98% (sodium + magnesium sulphate) immersion, whereas water immersion has the least values 10.96% and 14.35%. But iron content highest values noticed from atomic measurement analysis was sulphuric acid (8.15%) and sodium + magnesium sulphate (6.32%), also weight concentration followed the same pattern of 10.86% (sodium + magnesium sulphate) as the greatest value but next as sodium chloride at 8.66%, while both concentration scrutiny displayed lowest value of 10.96% and 14.35% respectively for sulphuric acid immersion. SEM analysis on binders was used to ascertain if the selected binders are pozzolans or not; while on alkaline activators is to differentiate the impact of alkaline elements on various compositions of the alkali-activated flyash GPC. SEM on binders materials revealed that each binder have Silicon dioxide ( $\text{SiO}_2$ ), Aluminumoxide ( $\text{Al}_2\text{O}_3$ ), and iron (III) oxide calcium as vital materials and lesser amount of  $\text{K}_2\text{O}$ ,  $\text{Fe}_2\text{O}_3$ ,  $\text{TiO}_2$ ,  $\text{MgO}$  and  $\text{SO}_3$ , which ascertain that the three binders are pozzolans. Whereas, SEM on hardened concrete was employed so as to know microstructure and durability characteristics of geopolymers concrete after immersion inside 5 different chemicals and water. Similarly, SEM on hardened concrete at 90 days shows that various chemicals used has little or no effect on pozzolanic contents and other materials in the fly ash-based geopolymer, but greatly affected by water immersion. Furthermore, the outcome of durability impact on the hardened concrete shows that various chemicals

used has little or no effect pozzolanic contents and other materials in the fly ash-based geopolymer, but greatly affected by water immersion i.e water immersion decreases the geopolymer contents. Similarly, these outcomes also confirm tremendous improvement observed in the values of flexural , compressive and split tensile strength of geopolymer concrete immersed in 4 different chemicals, while water was the least. These verdicts are in agreement with the result of silicon, alumina, calcium and iron as resolute by [Adbelli et al., \(2017\)](#); [Omotayo and Arum, \(2023\)](#); [Samantasinghar and Singh, \(2020\)](#); [Rui et al., \(2024\)](#) and [Arum et al., \(2022\)](#).

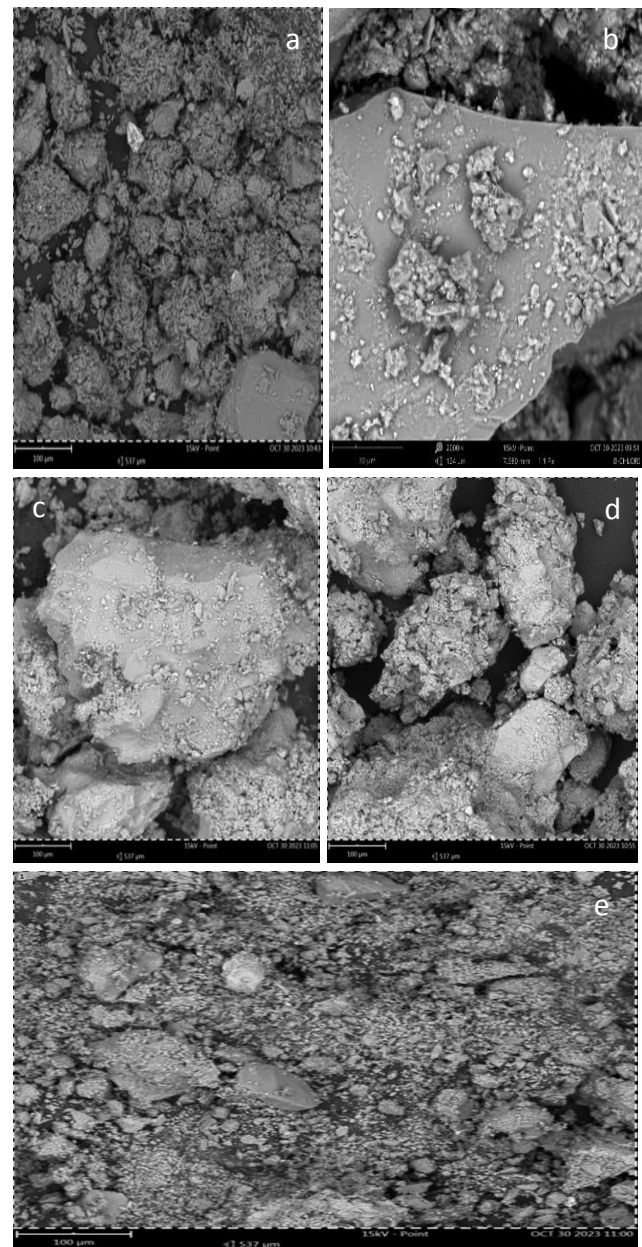


**Figure 7.** Outcome of GPC cured in (a) acid, (b) chloride and (c) water, (d) sulphate, and (e) magnesium immersion at 90 days.

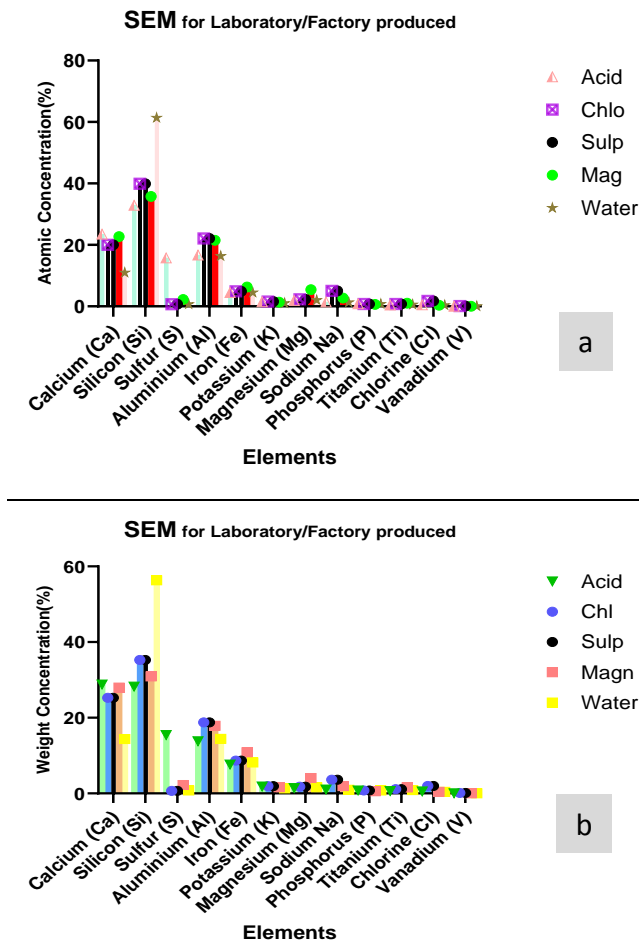


**Figure 8.** Outcome of SEM: a) Atomic concentration, and b) Weight concentration at 90 days.

**5) Outcome of partially replacement compressive experiment**

The compressive strength results for the various partially replaced geopolymer concrete are shown in Figures 9 and 10. The result shows that activation of cement based geopolymer reduces the compressive strength with increase in the percentage of cement with binders. However at 56 days, 7.5% partial replacement met the target strength of 1:1:5:3 mix ratio. Similarly, the compressive strength of the cement based geopolymer activated with 5% sodium silicate to reduce as the percentage of the binder increases. It is also observed that with the increase in the sodium silicate procured (i.e from 2.5% to 5% Na<sub>2</sub>SiO<sub>3</sub>), there was a gross increase in the compressive strength which led to the optimum percentage replacement to move from 7.5% to 12.5%. This indicate that the more the percentage addition of sodium silicate, the better the compressive strength for all the percentage replacement. The decrement in the compressive strength of the partially replaced fly ash-RHA geopolymer concrete owing to an imbalance of the Al/Si quotient, as binders contains slight quantity of alumina (Arum et al. 2022). On

the other hand, there could be an issue of dissolution of the silica extant in binders owing to lesser sodium hydroxide molar concentration as well as low temperature conditions of roughly 22–23 °C which would have stalled the polycondensation deeds of amorphous aluminosilicate GP products (Agashua et al., 2023; Phoo-ngernkham et al., 2017; Samantasinghar and Singh, 2020; Jindal and Sharma, 2020).

**6) Outcome of total replacement compressive experiment**

The result of the compressive strength at different days for the total replacement geopolymer concrete made from naturally made and procured sodium silicate are shown in Figures 11 and 12. Figures 10 and 11 shows that the naturally made sodium silicate increases the compressive strength as the temperature increases, with the optimum temperature of 70°C. The average compressive strength obtained at 70°C for the naturally made sodium silicate is 37.43N/mm<sup>2</sup>, which is 273.21% percentage increment when compared with the control with the compressive strength of 13.7N/mm<sup>2</sup>. Furthermore, the result of the procured sodium silicate shows an increment in the compressive strength of the geopolymer concrete as the temperature increases, even throughout the temperature variation from 25°C to 80°C. The average compressive strength obtained at 80°C for the procured sodium silicate is 31.03N/mm<sup>2</sup>, which is 226.5% percentage increment when compared with the control with the compressive strength of 13.7N/mm<sup>2</sup>. This is an indication that both the natural and the procured sodium silicate enhance the compressive strength of geopolymer concrete even more than double the control values. The behavior of the sodium silicate either procured or naturally made can probably be traced to the present aluminosilicates in the binders, which they help to polymerized. Similar result has also be reported in the literature that, addition of silicate source as an activator blended with hydroxide source will promote the condensation process of GPC (Adeshokan and Arum, 2023; Muhammad et al., 2019; Silva et al., 2020). The geopolymer concrete consists of super plasticizer (1.5%) and optimum of various binders i.e 5% FA + 7.5% KC + 10% RHA + aggregate + water at 7 and 14 days crushing for naturally made sodium silicate. The result shows that the naturally made sodium silicate increases the compressive strength as the curing temperature increases, with the optimum temperature still at 70°C. The average compressive strength obtained for 7 days at 70°C for the naturally made sodium silicate is 37.43N/mm<sup>2</sup>, which gave 248.54% percentage increment when compared with the 14 days compressive strength of 93.03N/mm<sup>2</sup>. The result indicates that the compressive strength of geopolymer concrete is a function of the curing days as well as curing temperature. The development of compressive strength at the various days was affected by the addition of the superplasticizer. However, the usage of superplasticizer

on the concrete strength must be limited to 1.5 because literature proves it that the optimum amount of

superplasticizer is 1.5 (Omotayo and Arum, 2022; Muhammad et al., 2020; Palcis, 2023; Dewi et al., 2018).

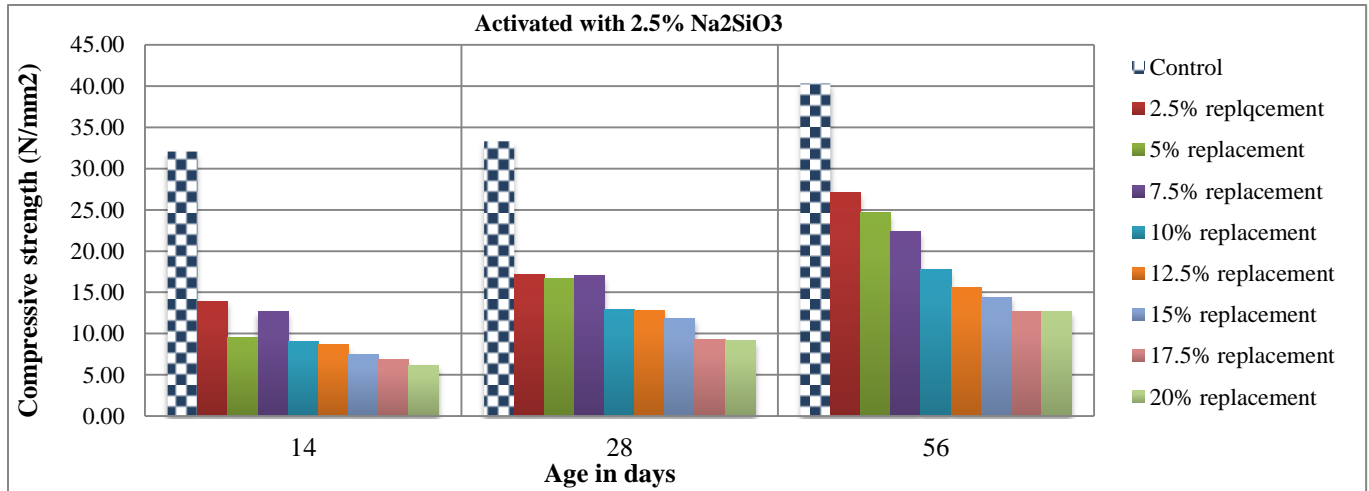


**Figure 9.** Compressive strength of partially replaced cement geopolymer concrete at different aging periods with 2.5% Na<sub>2</sub>SiO<sub>3</sub>.

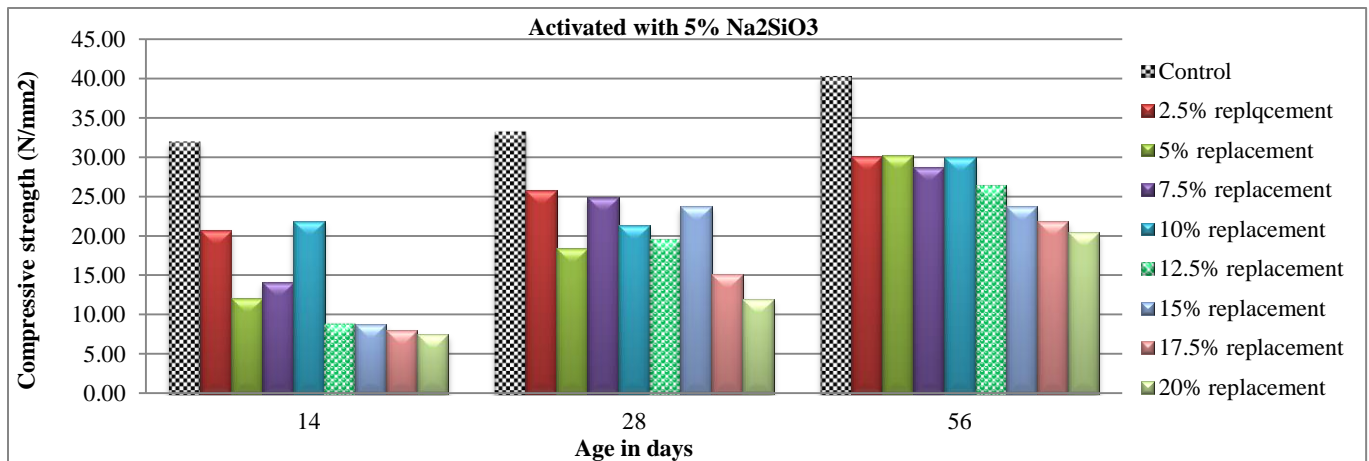


**Figure 10.** Compressive strength of partially replaced cement geopolymer concrete at different aging periods with 5% Na<sub>2</sub>SiO<sub>3</sub>.

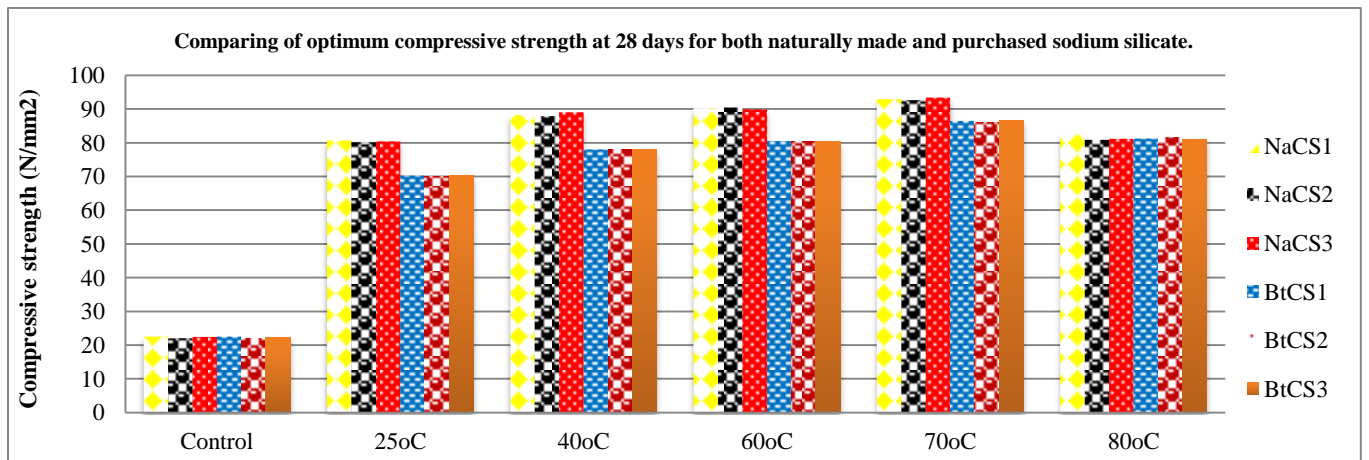


**Figure 11.** Optimum of Compressive strength at 28 days for various hot temperature. (Na: Naturally made sodium silicate; Bt: Purchased sodium silicate; CS: compressive strength).



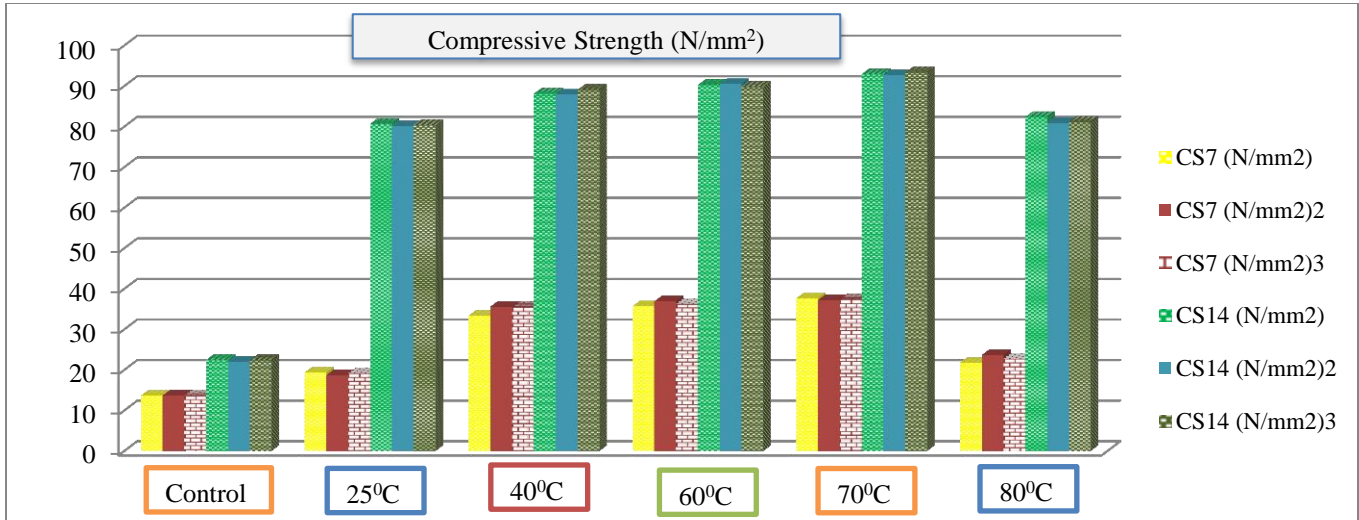


**Figure 12.** Compressive strength analysis outcome of varying temperature for 7 and 14 days (CS7: compressive strength at 7 days; CS14: compressive strength at 14 days)

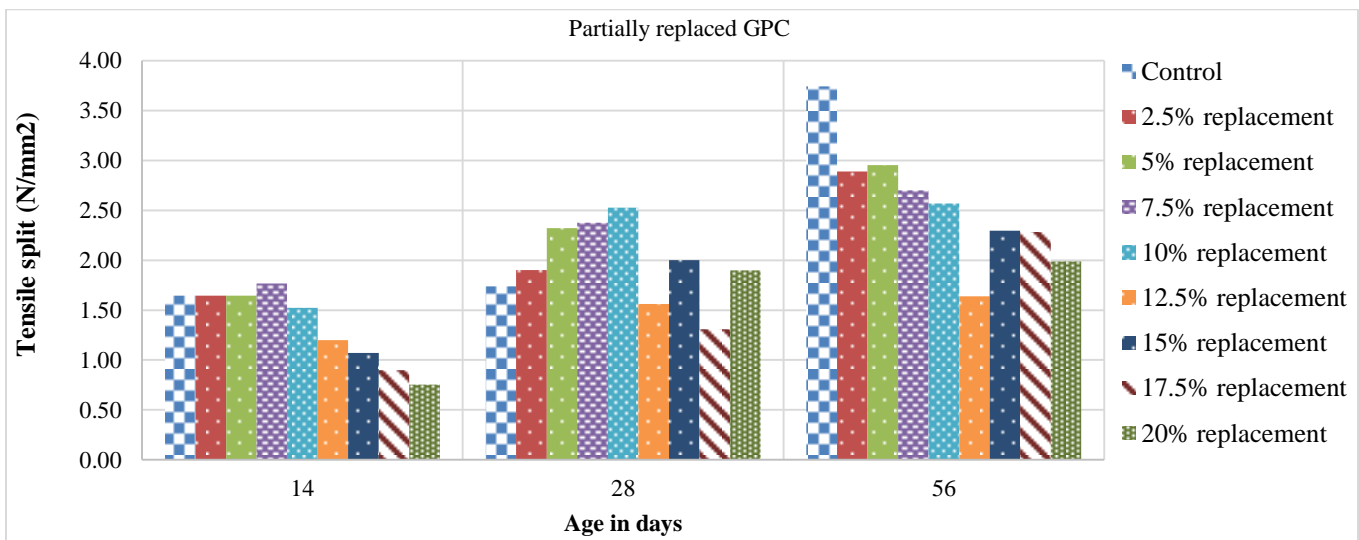


**Figure 13.** Split tensile strength test for activated fly ash based geopolymer.

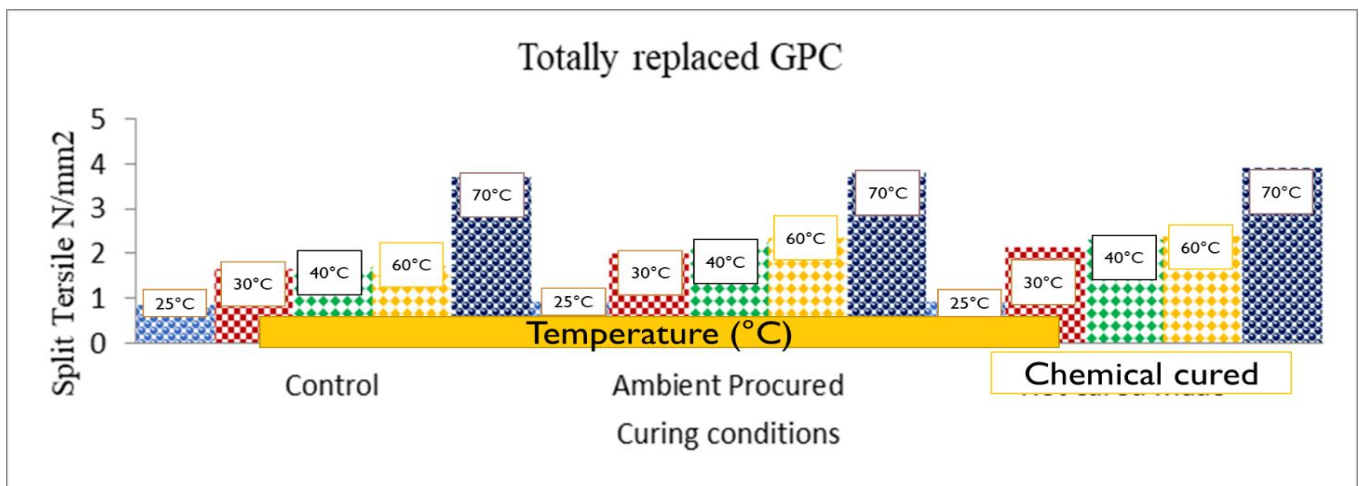


**Figure 14.** Split tensile strength test for activated fly ash based geopolymer. GPC = geopolymer concrete.

**7) Outcome of split tensile strength analysis**

The result of split tensile strength for the various partially and totally replaced geopolymer concrete are shown in Figures 13 and 14. Figure 13 demonstrated reduction in split tensile strength values as percentage replacement is increasing. While, as days increases totally replaced GP concrete increases as shown in Figure 14. Also, the outcome of totally replaced under differ different curing conditions displays that there is substantial increment on geopolymer concrete from naturally made sodium silicate with 1.1% percentage increment compared with control value of 0.87N/mm<sup>2</sup> at 7 days. Hence, using combine binders such as, kaolin clay and RHA to activate fly ash geopolymer substantially enhanced the totally replaced geopolymer concrete splitting tensile strength compared with partially replaced. Similar to compressive strength values, naturally made sodium silicate achieved higher splitting tensile strength values at different days of various hot-curing. It was ascertain from the experimental data that the indirect tensile values are at extreme compared to OPC for the mixes containing exact or beyond 30% replacement of cement with FA- KC - RHA. It was apparent that fly ash -RHA blended GPC specimens required at least of 13 h oven curing at 70<sup>0</sup>C temperatures (Bellium et al., 2019; Sing, 2018). Also, with the extra little quantities of Kaolin clay to FA-RHA based GPC, the oven curing can be avoided, and the desired strength, though below oven curing can be attained at ambient curing circumstances. It is evident that the increases of RHA content in the mixes the strength values were also increasing (Adeshokan and Arum, 2023; Obebe et al., 2023; Omotayo and Arum, 2022; Agashua and Ogbiye, 2018; Pelisser et al., 2021; Palcis, 2023). The highest splitting tensile strength was recorded when using GPC with 7.5% kaolin clay and 10% RHA with 5% fly ash content. Palcis (2023) had the same conclusion for Fly-ash based GPC.

**8) Porosity and sorptivity for optimum laboratory/factory produced with superplasticizer**

The outcome of porosity and sorptivity test for optimum laboratory/factory produced with superplasticizer is presented in Figures 15 and 16. Figure 15 reveals 5.2% and 4.7% at 70<sup>0</sup>C as the highest and 2.6% and 2.0% at 25<sup>0</sup>C as the lowest porosity values for laboratory and factory -produced sodium silicate GPC respectively. Whereas control highest value at 70<sup>0</sup>C was 2.8% and least value of 1.34% at 25<sup>0</sup>C. As temperature increases, porosity values both laboratory and factory-produced sodium silicate GPC enhanced, but reduce after 70<sup>0</sup>C.

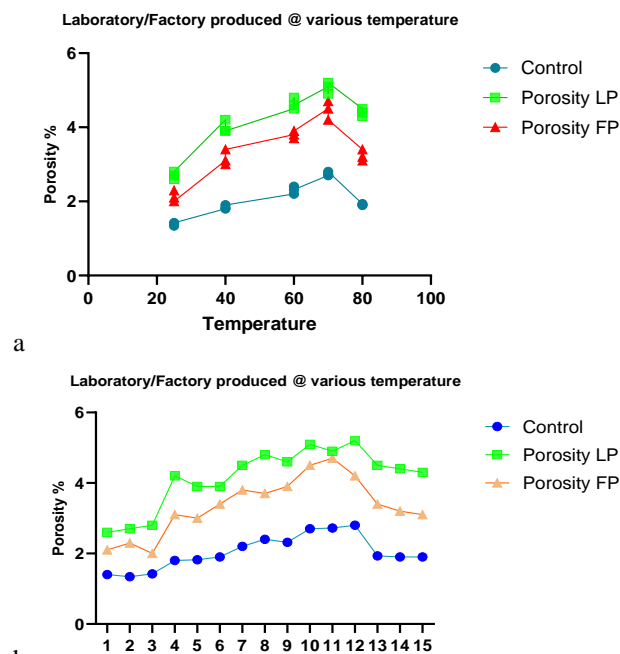


**Figure 15.** a) Varying temperature vs absorption, b).Absorption vs control of laboratory/factory-created sodium silicate.

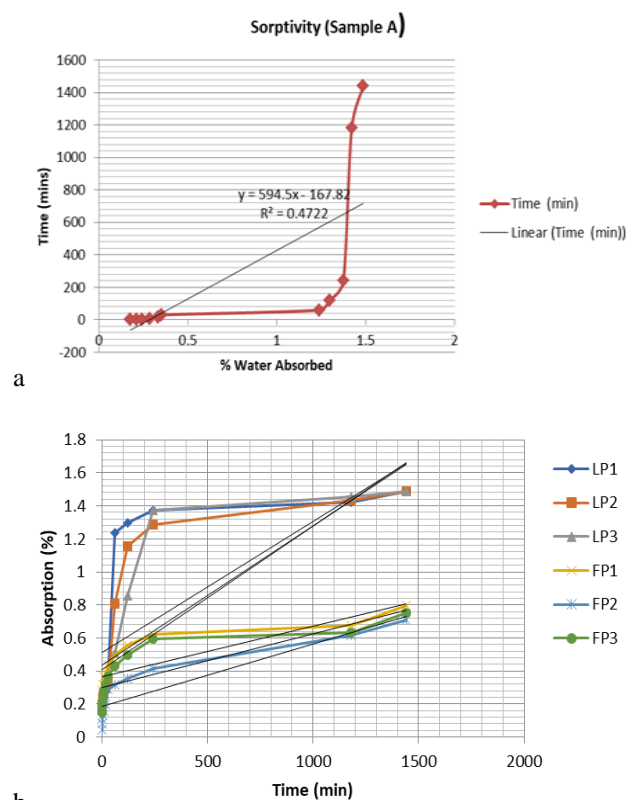


**Figure 16.** a) Sorptivity outcome of varying temperature and b) Outcome of varying temperature for optimum absorption level.

Sorptivity test (Figures 16) at initial time of 0.5min has the least water absorption values of 0.169019% and 0.044513%, and highest water absorption values of 1.487628% and 0.798575% at 1440mins for laboratory and factory-produced sodium silicate GPC respectively. As the time enhanced, absorption values also increases for both concrete. These results is in agreement with the totally replaced strength analysis result, which shows that as temperature enhances, GPC concrete strength amplifies. Pelisser et al., (2021), Cong and Cheng, (2021), and Dewi et al., (2018) had the same supposition for Fly-ash based GPC.

### 9) FA-based geopolymer concrete model formular

Two (Feret and Abram) models were utilized for the mixture proportion of concrete method and the outcome are display in Figures 17 and 18. P values, determination coefficient  $R^2$ , correlation coefficient R and the standard error are estimated so as to ascertain the accuracy of the Feret and regression model. Besides, there is need to known whether the variables are correlated and they are abridged in Table 3.

Regression analysis was done on the modified models to find the empirical constant of the best fit equation with a extreme  $R^2$  values and lowest loss function. Data pre-processing or normalization was carried out also, because the dataset has input values with varied scales. Thus, this approach accurately ascertains the minimum as well as maximum noticeable values, since redundant predictors can alter models precision and lead to unreliable predictions. Besides, the relation expressed formular from modified model used are represented in (Eqn 1 – 2). Eqn (1) was generalized from number of specimens (A, B, C, D and E) i.e independent variable, which are correlated to the Y (dependent variable). Thus, the correlation (Table 4) can be ascertain as diverse sets of experimental data points (dependent variables - Y1 to Y15) and (independent variable: A (A<sub>1</sub> to A<sub>15</sub>), B (B<sub>1</sub> to B<sub>15</sub>), C (C<sub>1</sub> to C<sub>15</sub>), D (D<sub>1</sub> to D<sub>15</sub>) and E (E<sub>1</sub> and E<sub>15</sub>). Whereas, constant K (K<sub>1</sub>, K<sub>2</sub>, K<sub>3</sub>, K<sub>4</sub> and K<sub>5</sub>) are proportionality coefficients between diverse Y and A - E values.

The resulting 28 days strength prediction model for flyash-based GPC mixes are summarized by the Eqn (2)

$$Y = [K1 (A)^{N1}]x [K2 (B)^{N2}]x [K3 (C)^{N3}] x$$

$$[K4 (D)^{N4}]x [K5 (E)^{N5}] \tag{1}$$

$$28 \text{ days} = -125.73 + 0.709 (7 \text{ days}) + 0.0324b + 0.056d \tag{2}$$

Where; d is density and b is binders (such as cement, flyash, rice husk ash and kaolin clay), Y is dependent variables, A to E is independent variables.

These models predicts compressive strength of conventional concrete from the concentration of cement in cement paste, which also include maximum paste thickness around aggregate particles and the effect of age of conventional concrete. Experimental results indicated that there is a strong relationship between the compressive strength of geopolymer concrete and the geopolymer binder concentration.

#### A) FA-based geopolymer concrete prediction process

As recommended by previous researcher such as Chouhan et al., (2018), Palcis, (2023) and Silva et al., (2020), the predictive performance of the Feret and Abram model is measured using the Mean Absolute Error (MAE), Mean Absolute Percentage Error (MAPE), Root Mean Squared Error (RMSE), Forecast Bias (B), and coefficient of determination ( $R^2$ ) metrics. The coefficient of determination ( $R^2$ ), which is calculated using Equations (3 and 4), and others through (Equations 5-7), are popular metric for evaluating models.

$$R^2 = 1 - [\sum_{i=1}^n (y_i - t_i)^2 \div \sum_{i=1}^n (t_i - \bar{t})^2] \tag{3}$$

$$R^2 = 1 - \{ \sum_{i=1}^n (Predicted_i - Actual_i)^2 - \sum_{i=1}^n (Actual_i - \bar{Actual})^2 \} \tag{4}$$

Where, *Predicted i* signifies the anticipated strength of *ith* sample, *Actuali* symbolizes the actual strength of *ith* sample and *Actual* exemplifies the mean of all samplings' actual strength.

*n* is the number of specimens, *ti* signifies observed outcomes, *yi* means projected outcomes, *t̄* is the sampling mean (i.e.,  $t = \sum_{i=1}^n t/n$ ).

$$MAPE = \frac{1}{N} \sum_{i=1}^n \{ |(Actual_i - Predicted_i) \div Actual_i| \} \times 100\% \tag{5}$$

$$RMSE = \sqrt{\frac{1}{N} \sum_{i=1}^n (Actual_i - Prediction_i)^2} \tag{6}$$

**Table 3.** FA-based GPC statistical analysis output

	Regression Statistics	Parameters		Coefficient		P-Value
Multiple R	0.99	Intercept		$b_0$	-125.7	0.00031
$R^2$	0.97	7 days CS	$X_1$	$b_1$	0.71	0.00011
Adjusted $R^2$	0.96	Binders	$X_2$	$b_2$	0.032	0.0133
Standard Error	1.58	Density	$X_3$	$b_3$	0.056	0.00021
Observations	94					
<b>ANOVA</b>	<b>df</b>	<b>SS</b>	<b>SH</b>	<b>F</b>	<b>Significance</b>	
Regression	3	3437.704	1145.65	455.65	0.0000	
Residual	23	55.251	2.513			
Total	26	3492.951				

**Style of silica, Alumina together with ratio of Al/si and Ca/(Si + Al)**

Combination	SiO <sub>2</sub>	Al <sub>2</sub> O <sub>3</sub> mol	Al/Si	Ca/(Si + Al)
A+B+C (1)	0.87	0.24	0.28	0.20
B+C+D (2)	0.83	0.23	0.28	0.35
C+D+E (3)	0.78	0.23	0.29	0.32
D+E+F (\$)	0.74	0.22	0.30	0.40

**Highpoints of the regression equations of the various experimental specimens.**

Classification of Mol samples	Linear regression equation
Al/Si, Correction Coefficient = 0.97 (12M, 7 days)	$y = 19.18 + 11.11x$
Al/Si, Corr. Coef = 0.98 (12M, 28 days)	$y = 15.10 + 7.57x$

**Statistical parameters and errors encounter during forecasting of the required Empirical model**

Models	MAE	RMSE	$R^2$	Bias
Feret	$2.392 \pm 0.21$	$3.459 \pm 0.35$	$0.959 \pm 0.01$	$0.648 \pm 0.47$
Abram	$2.343 \pm 0.26$	$3.854 \pm 0.50$	$0.957 \pm 0.01$	$0.139 \pm 0.18$

SS is sodium silicate; SH is sodium hydroxide and Mol is molarity, MAE is mean absolute error and RMSE is the root mean square error.

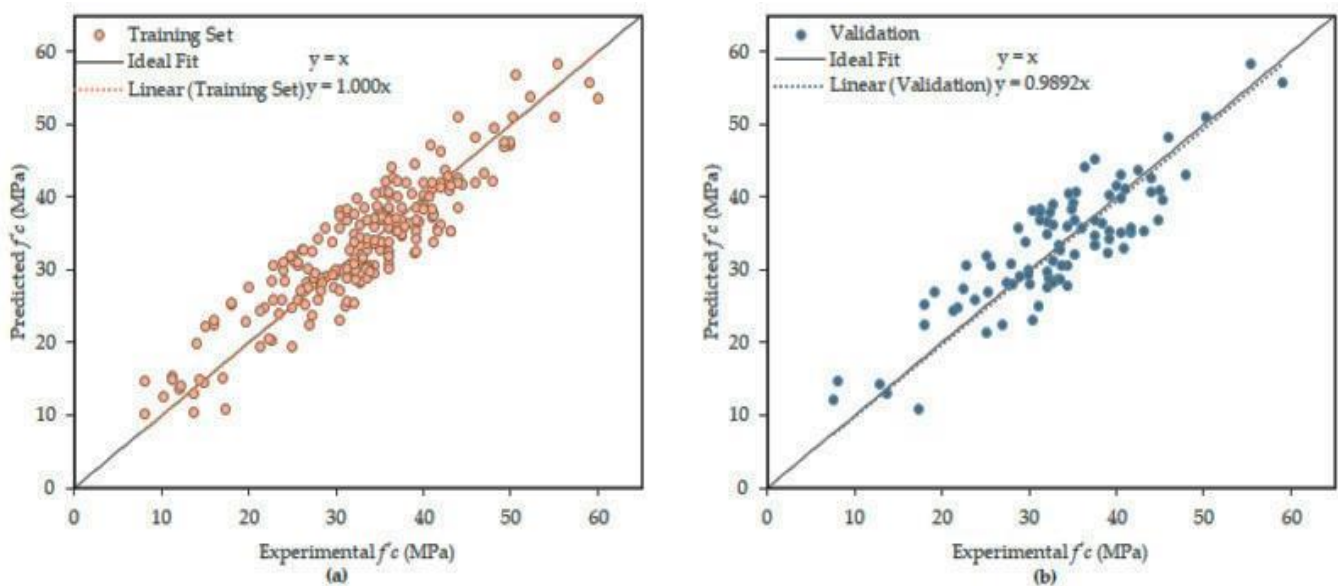


**Figure 17.** Experimental and forecasted values for compressive strength scrutiny: a) training and b) validation set values at various curing temperature.

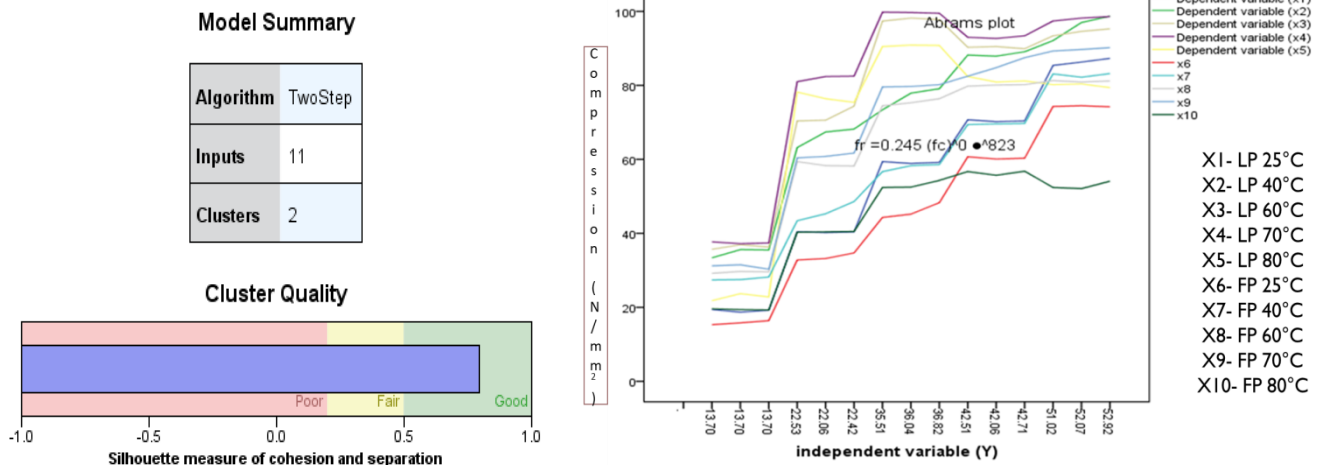


**Figure 18.** a) Model prediction cluster quality; b) independence vs dependence variable at various curing temperature. LP=Laboratory produce); FP=Factory produced.

**Table 4.** Dependent and independent variables (laboratory- produced GPC)

Sample ID	Various days	Control	25°C	40°C	60°C	70°C	80°C
		Y (dependent)	A (Independent)	B (Independent)	C (Independent)	D (Independent)	E (Independent)
A	ST7a	Y <sub>1</sub> (0.87)	A <sub>1</sub> (0.92)	B <sub>1</sub> (0.93)	C <sub>1</sub> (0.94)	D <sub>1</sub> (0.96)	E <sub>1</sub> (0.94)
A	ST7b	Y <sub>2</sub> (0.86)	A <sub>2</sub> (0.91)	B <sub>2</sub> (0.94)	C <sub>2</sub> (0.94)	D <sub>2</sub> (0.97)	E <sub>2</sub> (0.92)
A	ST7c	Y <sub>3</sub> (0.86)	A <sub>3</sub> (0.93)	B <sub>3</sub> (0.93)	C <sub>3</sub> (0.95)	D <sub>3</sub> (0.96)	E <sub>3</sub> (0.93)
B	ST14a	Y <sub>4</sub> (1.65)	A <sub>4</sub> (2.02)	B <sub>4</sub> (2.04)	C <sub>4</sub> (2.07)	D <sub>4</sub> (2.15)	E <sub>4</sub> (2.09)
B	ST14b	Y <sub>5</sub> (1.65)	A <sub>5</sub> (2.02)	B <sub>5</sub> (2.05)	C <sub>5</sub> (2.09)	D <sub>5</sub> (2.14)	E <sub>5</sub> (2.08)
B	ST14c	Y <sub>6</sub> (1.66)	A <sub>6</sub> (2.03)	B <sub>6</sub> (2.04)	C <sub>6</sub> (2.08)	D <sub>6</sub> (2.16)	E <sub>6</sub> (2.07)
C	ST21a	Y <sub>7</sub> (1.69)	A <sub>7</sub> (2.23)	B <sub>7</sub> (2.25)	C <sub>7</sub> (2.28)	D <sub>7</sub> (2.32)	E <sub>7</sub> (2.12)
C	ST21b	Y <sub>8</sub> (1.68)	A <sub>8</sub> (2.24)	B <sub>8</sub> (2.26)	C <sub>8</sub> (2.29)	D <sub>8</sub> (2.31)	E <sub>8</sub> (2.20)
C	ST21c	Y <sub>9</sub> (1.69)	A <sub>9</sub> (2.22)	B <sub>9</sub> (2.25)	C <sub>9</sub> (2.27)	D <sub>9</sub> (2.33)	E <sub>9</sub> (2.19)
D	ST28a	Y <sub>10</sub> (1.73)	A <sub>10</sub> (2.35)	B <sub>10</sub> (2.37)	C <sub>10</sub> (2.39)	D <sub>10</sub> (2.40)	E <sub>10</sub> (2.21)
D	ST28b	Y <sub>11</sub> (1.72)	A <sub>11</sub> (2.36)	B <sub>11</sub> (2.38)	C <sub>11</sub> (2.4)	D <sub>11</sub> (2.43)	E <sub>11</sub> (2.19)
D	ST28c	Y <sub>12</sub> (1.73)	A <sub>12</sub> (2.34)	B <sub>12</sub> (2.38)	C <sub>12</sub> (2.42)	D <sub>12</sub> (2.44)	E <sub>12</sub> (2.18)
E	ST56a	Y <sub>13</sub> (3.33)	A <sub>13</sub> (3.31)	B <sub>13</sub> (3.34)	C <sub>13</sub> (3.41)	D <sub>13</sub> (3.91)	E <sub>13</sub> (3.02)
E	ST56b	Y <sub>14</sub> (3.34)	A <sub>14</sub> (3.30)	B <sub>14</sub> (3.36)	C <sub>14</sub> (3.42)	D <sub>14</sub> (3.90)	E <sub>14</sub> (3.04)
E	ST56c	Y <sub>15</sub> (3.36)	A <sub>15</sub> (3.29)	B <sub>15</sub> (3.35)	C <sub>15</sub> (3.43)	D <sub>15</sub> (3.92)	E <sub>15</sub> (3.03)

$$MAE = \frac{1}{N} \sum_{i=1}^N |Actual_i - Predicted_i| \quad (7)$$

The value of  $R^2$  is not up to 1 with 1 signifying model perfect fit. The horizontal axis is the observed strength and the vertical axis symbolizes the strength anticipated by the Feret model. In all, the data points that were clustered near the diagonal line for both test as well as training sets, demonstrating that the model provides precise values of the compressive strength (Figure 17a). Further, series of machine learning predictive models were then employed to predict the compressive strength of geopolymers

concrete with laboratory-produced sodium silicate and hydroxide alkaline as activator (Figure 17b). These regression predictive techniques were divided into three main categories which are trees, Gaussian and Support Vector Machine techniques together with linear regression using the regression learner application in Matlab version 2022. Their performance were also rated using the Root Mean Square Error (RMSE), Mean Square Error (MSE), Mean Absolute Error (MAE) and R-square error indices, the lower the result of these performance indices. Figure 17c shows that the difference between the true and

predicted was minimal for all except one of the plot which shows good predictive returns. Likewise, more of the errors are close to the zero residual line, showing positive returns in error minimization and good predictive performances. It is perceived that the anticipated formulation gives close results to the experimental data and the usage of alkali solution ratios in the creation of geopolymer concrete enhances the calculated values statistically.

### **B) Performance, void ratio, extended micro cracks and reliability impact of FA-based geopolymer concrete**

The performance of flyash-RHA based GPC can be improve through addition of moderate amount of kaolin clay and 1.5% laboratory produced superplasticizer, so as to solve problem of hot curing and workability issues associated with it. For this type of flyash-RHA geopolymer concrete (FRGPC), the workability enhanced from the production to the concrete placement time and minimal slump loss ensued over 2 hours (in contrast with ordinary Portland cement (OPC) concrete. Besides, with strain gauge embedded techniques there is little initial in situ expansion and tensile stain growth till 14 day. But at 90 days OPC concrete cracked but FRGPC concrete remain uncracked. This behavior can be as a result of higher tensile strain capability of FRGPC than OPC concrete created through higher creep and lesser elastic modulus. Reliability of the expected performance of flyash-RHA GPC is evaluated through various methodologies based on Ferret, linear regression and specialized reliability software package. Reliability methodologies that were considered comprised full coupling with an Feret and Abram modified equations and surface response centered approaches together with first order reliability techniques or importance sampling approach.

### **C) Geopolymerization, thermal conductivity and stability of FA-based geopolymer concrete**

Flyash-RHA based GPC have unveiled significant resistance to higher temperatures with addition of moderate amount of kaolin during production, as verified in the laboratory against cracking, durability and strength degradation. At optimum curing temperature of 60°C for metakaolin based geopolymers shows the best mechanical and physical properties. This is an indication that below or above 60°C curing temperature greatly affect metakaolin based geopolymers adversely. While, FRGPC activated with pure kaolin trend is as curing days increases both factory-produced and laboratory-produced geopolymer

concrete increases, with the optimum temperature at 70°C. Also, Thermal conductivity (k-value) which is a material's property that ascertains its heat conduction ability reveals that FA-RHA based GPC was below that of control (OPC) concrete. So as to simulate heat transfer via the GPC, the thermal diffusivity was computed, via 500 × 500 mm OPC as control and flyash-RHA GPC (partial and pure GPC). The outcome shown an extremely small thermal conductivities of 100% laboratory-created sodium silicate fly ashes- RHA geopolymer (LCSSFRGP) concrete, ranging from 0.048 to 0.087 W/mK, advocate for a possible usage of LCSSFRGP for thermal insulation, for instance fireproofing materials. Besides, witnessed results proved that the thermal conductivity of LCSSFRGP concrete almost linearly reduced as cement content increased whereas the discrepancy of thermal conductivity of LCSSFRGP concrete caused by ambient temperature was relatively low. Furthermore, the thermal conductivity of LCSSFRGP concrete was lesser than that of factory-created geopolymer concrete.

Flyash-RHA GPC can considerably enhance the thermal stability of geopolymers, i.e with optimum of various binders of 5% FA + 7.5% KC + 10% RHA + 1.5% superplasticizer aggregate + water, the better thermal stability were between 700°C to 900°C.

## **CONCLUSION**

This research discusses experimental studies of locally made super-plasticizer geopolymer concrete. SEM and FTIR reveal clearly that all the binders selected have calcium, alumina and silica as vital materials and others in lesser quantities. Strength test for partially replaced cement GPC at different curing days up to 56 days, signifies that up to 10% replacement of other binders the compressive strength increases. While optimum for naturally made super plasticizer were 1.5% and various binders as 5% FA + 7.5% KC + 10% RHA + aggregate + water for both naturally made and readymade sodium silicate. The result also shows that as hot temperature increases both compressive strength increases, while the weight of GPC was decreases till 70°C. There is reduction in split tensile strength values as percentage replacement is increasing, but for totally replaced GP as days increases split tensile strength values increases. This indicate that the more the percentage addition of sodium silicate, the better the strength for total percentage replacement. Likewise, durability impact on the hardened concrete shows that various chemicals used except water has little or no effect on pozzolanic contents and other materials in

the fly ash-based geopolymer, It can be concluded that geopolymer concrete made from rice husk ash, fly ash and kaolin clay with combination of alkaline activator from both natural and factory-produced sodium silicate are good material for high performance concrete. Finally, linear regression, Feret and Abrams modeling shows that the difference between the true and predicted was minimal, which indicate good predictive returns.

## DECLARATIONS

### Corresponding Author

Correspondence and requests for materials should be addressed to Lucia Omolayo Agashua; agashualight@gmail.com; ORCID: 0000-0002-5262-5710.

### Data availability

The datasets used and/or analysed during the current study available from the corresponding author on reasonable request.

### Acknowledgements

The authors would like to acknowledge the Nigerian Building and Road Research Institute (NBRI) Jabi Abuja, Federal Ministry of Works, concrete and pavement unit Sheda Abuja laboratories and Chemical and Material Engineering laboratory, Umaru Musa Yaradua University Dutsin Ma, Kastina. for creating a conducive environment to conduct this research.

### Authors' contribution

Agashua LO performed the experiments, Agashua LO, Arum C and Ikumapayi CM analysed the data obtained and wrote the manuscript. Arum C and Oluyemi-Ayibowu designed the experimental process and revised the manuscript. All the authors read and approved the final manuscript.

### Competing interests

The authors declare no competing interests in this research and publication.

## REFERENCES

- Abdelli K, Tahlaïti M and Oudjit MN. (2017). Influence of the origin of metakaolin on pozzolanic reactivity of mortars Energy Procedia.139(2), 230-235. Available at: <https://doi.org/10.1016/j.egypro.2017.11.201>
- Adeshokan M and Arum C. (2023). Comparison between the Compressive Strength of Binary and Ternary Alkaline activated Pozzolanic Concrete. J. Appl. Sci. Environ. Manage., 27 (1), 747-752. Available at: <https://dx.doi.org/10.4314/jasem.v27i4.15>
- Agashua LO, Ogiye AS, Amu OO, Oluyemi-Ayibowu BD, Igibah CE and Onakunle O. (2023). Grapher Analysis and the Impact of Sodium Silicate Activator on Strength of Kaolin-rice husk ash stabilized laterite. Materials Today Proceedings, 74 (2), 377-388. Available at: <https://doi.org/10.1016/j.matpr.2022.09.171>
- Agashua LO and Ogiye AS. (2018). Influence of Cement, Bitumen and Lime on Some Lateritic Soil Samples as Pavement Material. ICESW IOP Publishing. IOP Conf. Series: Materials Science and Engineering 413 (1), 1-13. Available at: <https://doi.org/10.1088/1757-899X/413/1/012012>
- Arum C, Akande SP and Alabi SA. (2022). Strength Evaluation of Pozzolanic Concrete Containing Calcined Ceramic Waste And Glass Waste Powder. Journal of Engineering and Engineering Technology 16(1), 113-119. Available at: <https://doi.org/10.51459/futajeet.2022.16.1.420>
- Babatola O and Arum C. (2020). Determination of the Compressive Strength of Concrete from Binary Cement and Ternary Aggregates. Open Journal of Civil Engineering 10(4), 385 - 402. Available at: <https://doi.org/10.4236/ojce.2020.104029>
- Bellum RR, Nerella R, Madduru SRC and Indukuri CSR. (2019). Mix design and mechanical properties of fly ash and GGBFS-synthesized alkali-activated concrete (AAC). *Infrastructures*, 4(2): 20-29. Available at: <https://doi.org/10.3390/infrastructures4020020>
- Chouhan R.K, Mudgal M, Bisarya A and Srivastava A.K. (2018). Rice-husk-based superplasticizer to increase performance of fly ash based geopolymer concrete. Emerging Materials Research, 7(3), 1-32. Available at: <https://doi.org/10.1680/jemmr.18.00035>
- Cong P and Cheng Y. (2021). Advances in geopolymer materials: A comprehensive review. Journal of Traffic and Transportation Engineering (English Edition), 8(2), 1-12. Available at: <https://doi.org/10.1016/j.jtte.2021.03.004>
- Dewi R, Agusnar H, Alfian Z and Tamrin T. (2018). Characterization of technical kaolin using XRF, SEM, XRD, FTIR and its potentials as industrial raw materials. Journal of Physics Conference Series, 1116(4), 11-23. Available at: <https://doi.org/10.1088/1742-6596/1116/4/042010>
- Faluyi F, Arum C, Ikumapayi CM and Alabi SA. (2021). Review of the Compressive Strength Predictor Variables of Geopolymer Concrete. FUOYE Journal of Engineering and Technology, 7(3), 1-11. Available at: <https://doi.org/10.46792/fuoyejet.v7i3.884>
- Hassan A, Arif M and Shariq M. (2019). Effect of curing condition on the mechanical properties of fly ash-based geopolymer concrete. SN Appl Sci., 1(2), 1694 – 1707. Available at: <https://doi.org/10.1007/s42452-019-1774-8>
- Jindal BB and Sharma R. (2020). The effect of nano materials on properties of geopolymers derived from industrial byproducts: a state-of-the-art review. Construction and Building Materials, 252(1), 119-128. AVAILABLE AT: <https://doi.org/10.1016/j.conbuildmat.2020.119028>

- Obebe MD, Ikumapayi CM and Alaneme KK. (2023). Structural performance evaluation of concrete mixes containing recycled concrete aggregate and calcined termite mound for low-cost housing. *Alexandria Engineering Journal* 72(2), 237–346. Available at: <https://dx.doi.org/10.1016/j.aej.2023.03.095>
- Omotayo OO and Arum C. (2022). Challenges and Prospects of Widespread Adoption of Pozzolans for Building Construction: A Statistical Assessment. *International Journal of Engineering*. 35(10):1929-1940. Available at: <https://doi.org/10.5829/ije.2022.35.10a.12>
- Muhammad NS, Hadi I and Shelley P. (2019). Optimum mix design of geopolymer pastes and concretes cured in ambient condition based on compressive strength, setting time and workability. *Journal of Building Engineering*, 23(2), 301-313. Available at: <https://doi.org/10.1016/j.jobe.2019.02.006>
- Palcis RP. (2023). The Effect of Water Quality on Concrete Strength and Permeability: A Review of the Use of Chlorinated Water vs. Top Water in Concrete Mix Design. 2(1), 1-10. Available at: <https://doi.org/10.13140/RG.2.2.29845.81126/1>
- Pelisser F, Bernardin A.M and Michel M.D. (2021). Compressive strength, modulus of elasticity and hardness of geopolymeric cement synthesized from non-calcined natural kaolin. *Journal of Cleaner Production*. 280 (1), 124-136. Available at: <https://doi.org/10.1016/j.jclepro.2020.124293>
- Phoo-ngernkham T, Hanjitsuwan S, Damrongwiriyanupap N and Chindaprasirt P. (2017). Effect of sodium hydroxide and sodium silicate solutions on strengths of alkali activated high calcium fly ash containing Portland cement. *KSCE J.Civ. Eng.*, 21(6), 2202–2210. Available at: <https://doi.org/10.1007/s12205-016-0327-6>
- Rui L, Jizhao L, Huigang X, Da Y, Wenwei Y. (2024). Chloride ion diffusion performance of concrete and its influence on scour resistance. *Structures*, 60 (1), 105789. Available at: <https://doi.org/10.1016/j.istruc.2023.105789>
- Samantasinghar S and Singh S. (2020). Effects of curing environment on strength and microstructure of alkali-activated flyash-slag binder. *Construction and Building Materials*. 235(2), 117481. Available at: <https://doi.org/10.1016/j.conbuildmat.2019.117481>
- Shill SK, Al-Deen S and Ashraf M. (2020). Resistance of fly ash based geopolymer mortar to both chemicals and high thermal cycles simultaneously. *Construction and Building Materials* 239(2), 117886. Available at: <https://doi.org/10.1016/j.conbuildmat.2019.117886>
- Silva G, Kim S and Aguilar R. (2020) Natural fibers as reinforcement additives for geopolymer a review of potential eco-friendly applications to the construction industry. *Sustainable Materials and Technologies* 23(1), 42-56. Available at: <https://doi.org/10.1016/j.susmat.2019.e00132>
- Tutal, A, Partschefeld, S., Schneider, J., and Osburg, A. (2020). Effects of Bio-Based Plasticizers, Made From Starch, on the Properties of Fresh and Hardened Metakaolin-Geopolymer Mortar. *Geopolymer*, 68(1), 413–427. Available at: <https://doi.org/10.1007/s42860-020-00084-8>

**Publisher's note:** [Scienceline Publication](#) Ltd. remains neutral with regard to jurisdictional claims in published maps and institutional affiliations.



**Open Access:** This article is licensed under a Creative Commons Attribution 4.0 International License, which permits use, sharing, adaptation, distribution and reproduction in any medium or format, as long as you give appropriate credit to the original author(s) and the source, provide a link to the Creative Commons licence, and indicate if changes were made. The images or other third party material in this article are included in the article's Creative Commons licence, unless indicated otherwise in a credit line to the material. If material is not included in the article's Creative Commons licence and your intended use is not permitted by statutory regulation or exceeds the permitted use, you will need to obtain permission directly from the copyright holder. To view a copy of this licence, visit <https://creativecommons.org/licenses/by/4.0/>.